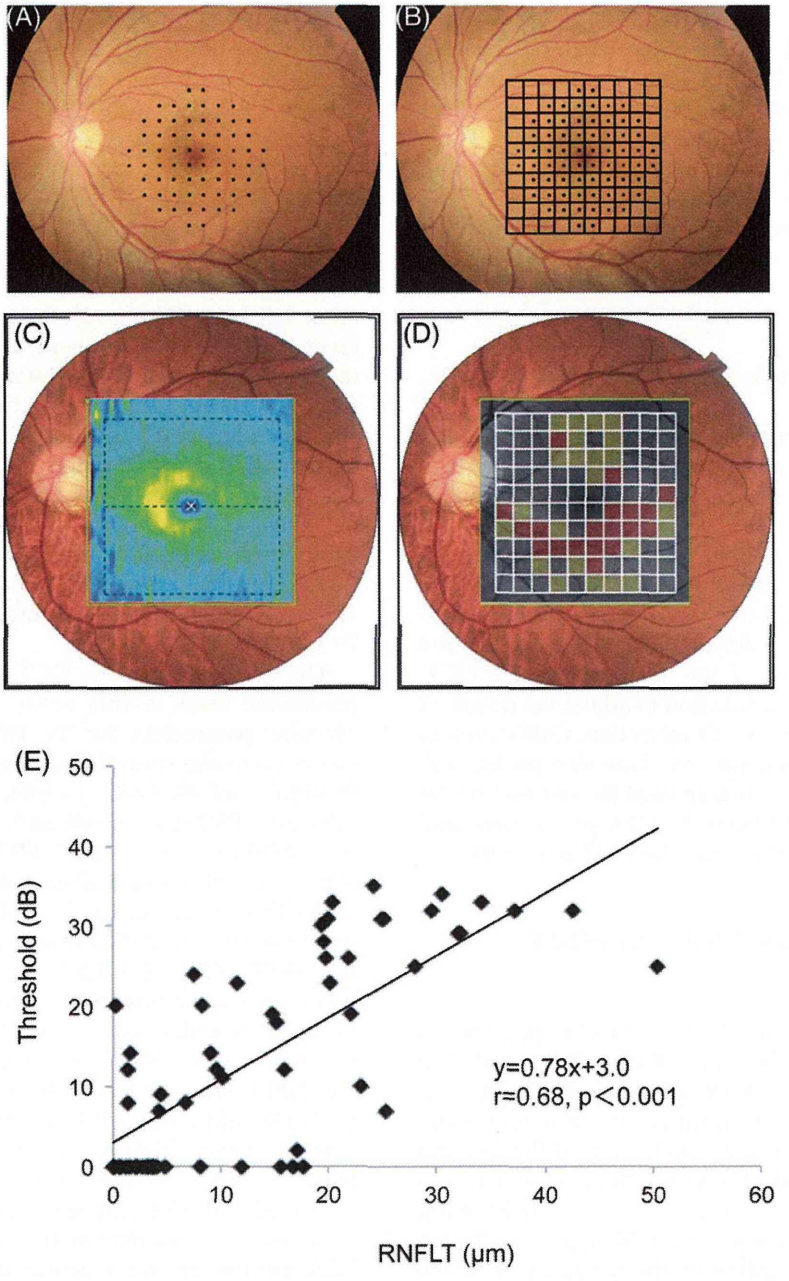

FIGURE 1 Correspondence for 68 HFA 10-2 test points from and 10 × 10 3D OCT-2000 grids. (A) All 68 HFA 10-2 test points. (B) One to one correspondence between each HFA 10-2 test point and a 10 × 10 3D OCT-2000 grid from. (C) 3D OCT-2000 map of the RNFL, GCC and GCL + IPL in the macula. (D) Significance map of macular thickness. (E) Blot graph showing the correlation between measured OCT thickness and threshold values, with the formula of linear regression analysis for each test point.

TABLE 1 Demographic data for the glaucoma patients in this study.

Sex Male: Female	43(72%) : 17(28%)
Age (yrs)	65.7 ± 11.1
Spherical equivalent (D)	−2.8 ± 2.2
Visual acuity (logMAR)	0.08 ± 0.28
MD of HFA30-2(dB)	−12.1 ± 8.9
Pretreated IOP (mmHg)	19.7 ± 7.1
cpRNFLT(μm)	79.3 ± 14.8

was lowest in the upper nasal area. There was a significant correlation between GCC and PD ($r = 0.28$–0.65) in all but seven test points (Figure 2F). The correlation coefficient with PD was lower than that with threshold or TD.

The thickness of the GCL + IPL was significantly correlated with the threshold ($r = 0.26$–0.81), TD ($r = 0.27$–0.81) and PD ($r = 0.24$–0.59) in the central circular area (Figure 2G–I). Peripheral test points, however, showed no significant correlation between

TABLE 2 The relationship between the thickness of each macular retinal layer and clinically-measured parameters.

	RNFL		GCC		GCL+IPL	
	r	*p*	*r*	*p*	*r*	*p*
MD(HFA30-2)	**0.49**	**<0.001**	**0.44**	**<0.001**	**0.33**	**0.013**
PSD(HFA30-2)	**−0.49**	**<0.001**	**−0.37**	**0.005**	−0.22	0.09
MD(HFA10-2)	**0.76**	**<0.001**	**0.72**	**<0.001**	**0.55**	**<0.001**
PSD(HFA10-2)	−0.17	0.21	0.06	0.67	0.18	0.17
logMAR	**−0.35**	**0.008**	**−0.41**	**0.002**	**−0.39**	**0.003**
cpRNFLT (μm)	**0.34**	**0.009**	**0.33**	**0.013**	**0.31**	**0.021**
Spherical equivalent (D)	0.09	0.50	0.08	0.54	0.09	0.50
preIOP (mmHg)	0.12	0.39	0.06	0.65	−0.02	0.91

The data (correlation coefficient value and *p* value) are described in each column.
Values in bold are statistically significant.

structure and function for threshold, TD, or PD (Figure 2G–I).

In this way, we established the correlation formula between macular OCT parameters and HFA 10-2 results for each test point. We then used the inverse calculation of the correlation formulas for each of the 68 test points to create an OCT parameter-derived simulation of the sensitivity of the visual field. We validated the simulated visual fields with an additive data set from the patients.

First, we compared the average simulated visual field sensitivity with real measured HFA 10-2 parameters (threshold, TD and PD) in the study group. There was a significant correlation between the averaged simulated visual fields and the real visual sensitivity mean, as shown in Table 3. The simulation produced from RNFLT data showed a significant correlation to the real average threshold ($r = 0.76$), TD ($r = 0.77$) and PD ($r = 0.31$). The simulation produced from GCC data showed a significant correlation to the real average threshold ($r = 0.72$) and TD ($r = 0.73$), but not to PD ($r = 0.12$). The simulation produced from GCL + IPL data showed a significant correlation to the real average threshold ($r = 0.56$) and TD ($r = 0.56$), but not to PD ($r = 0.08$).

Next, we validated the simulated visual fields with an additive data set of 29 other glaucoma patients. The demographic data for these patients are listed in Table 4. The average age of the patients was 65.7 ± 11.1 years, average spherical equivalent was -2.8 ± 2.2 diopters, average logMAR visual acuity was 0.084 ± 0.28, average HFA 30-2 MD was -12.1 ± 8.9 dB, average pretreated IOP was 18.3 ± 3.5 mmHg and average cpRNFLT was 79.3 ± 14.8 μm.

We were able to find a significant correlation between the average from the simulated visual fields and the real measured mean of visual fields parameters, as shown in Table 5. The simulation created from RNFLT data was also significantly correlated with real average threshold values ($r = 0.87$, $p < 0.001$), as well as TD ($r = 0.86$, $p < 0.001$) and PD values ($r = 0.64$, $p < 0.001$). The simulation created from GCC data showed a significant correlation to real average threshold values ($r = 0.78$, $p < 0.001$), as well as TD ($r = 0.77$, $p < 0.001$), but not to PD values ($r = 0.35$, $p = 0.067$). The GCL + IPL-derived simulation showed significant correlation to real average threshold values ($r = 0.63$, $p < 0.001$), as well as TD ($r = 0.62$, $p < 0.001$), but not PD values ($r = 0.22$, $p < 0.254$). We constructed a simulated grayscale visual field from RNFL with ten shades of gray representing 5 dB steps, as shown in Figure 3.

DISCUSSION

In this study, our results showed structure and function to be significantly correlated in the macular area. The correlation maps for RNFL, GCC and GCL + IPL had characteristic variations; the map for RNFL displayed a higher correlation coefficient with average visual sensitivity. We created a simulated visual field with an inverse calculation and the correlation formula for macular OCT thickness in each layer and the parameters from the HFA 10-2 program. We found that the simulation was significantly correlated with real results from the HFA 10-2 program. We therefore believe that simulated visual fields produced from OCT macular map data may have a real and valuable use in a routine clinical setting.

We found that the sensitivity of the macular visual field had a different correlation coefficient for each retinal layer. There was a higher correlation between HFA average threshold and RNFLT than thickness of GCC or GCL + IPL. Each layer of the retina contains a different section of the ganglion cells. The RNFL contains the axons and the GCL + IPL contains the cell bodies and dendrites, while the GCC contains all parts. Degeneration of the axons and dendrites has been detected in glaucoma patients.[14] After axons degenerate, microglia phagocyte the resulting debris and the thickness of the RNFL immediately decreases. These data suggest that axonal loss in RGCs may be better correlated to functional deterioration than it is to cell body loss in the macular area.

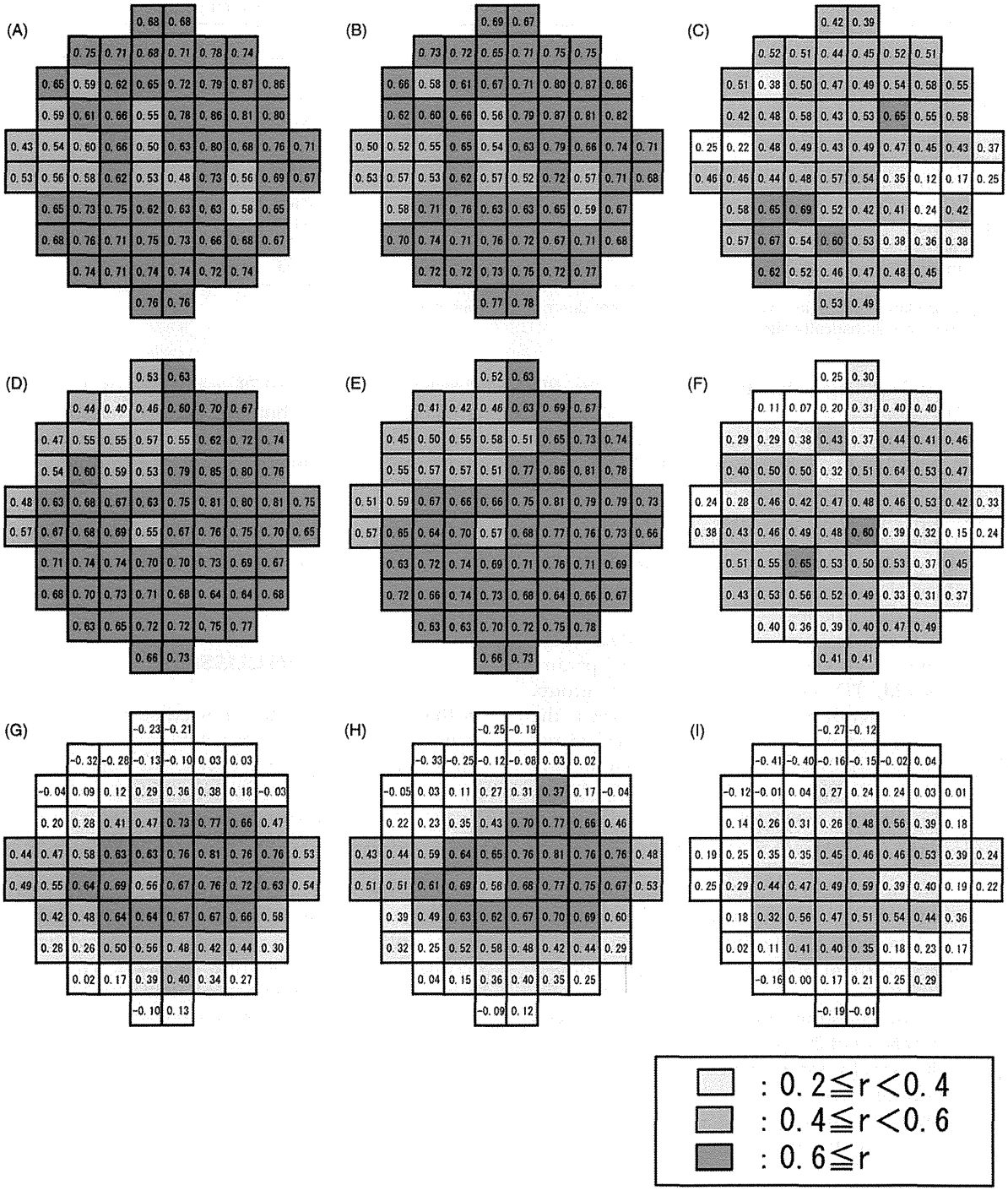

FIGURE 2 Distribution of the correlation coefficient for RNFLT, GCC, GCL + IPL and HFA 10-2 parameters in all 68 test points. Distribution grayscale maps showing the correlation coefficient for RNFLT (A–C), GCC (D–F) and GCL + IPL (G–I). Left panel (A, D, G) showed the threshold. Left side of figures was nasal side. Central panel (B, E, H) showed TD. Right panel (C, F, I) showed PD. Darker shades of gray indicate a higher correlation coefficient, with a step scale of 0.2. The white column indicates no statistical significance.

Our results showed a characteristic distribution of the correlation coefficient. The correlation between RNFLT and each HFA parameter in the overall nasal visual field was weaker than the correlation between the GCC and each HFA parameter in the upper nasal visual field. The nasal area is known to be a common site of glaucomatous visual field loss, and the threshold in this area can easily reach zero. OCT measurements of retinal layer thickness never reach zero, however, due to the presence of astrocytes and

TABLE 3 The relationship between VFs simulated from different macular maps and HFA 10-2 parameters.

	Calculated VF value					
	from RNFL		from GCC		from GCL+IPL	
	R	*p*	*r*	*p*	*r*	*p*
Measured mean of threshold	**0.76**	**<0.001**	**0.72**	**<0.001**	**0.56**	**<0.001**
Measured mean of TD	**0.77**	**<0.001**	**0.73**	**<0.001**	**0.56**	**<0.001**
Measured mean of PD	**0.31**	**0.016**	0.12	0.35	0.08	0.57

Values in bold are statistically significant.

TABLE 4 Demographic data for additive glaucoma patients used to validate the simulation.

Sex Male: Female, *n* (%)	16 (55%):13 (45%)
Age (yrs)	60.8 ± 9.0
Spherical equivalent (D)	−4.2 ± 2.9
Visual acuity (logMAR)	0.003 ± 0.11
MD of HFA30-2 (dB)	−17.2 ± 8.4
Pretreated IOP (mmHg)	18.3 ± 3.5
cpRNFLT (μm)	74.8 ± 13.7

TABLE 5 The relationship between HFA 10-2 parameters and simulated VFs produced from different macular maps.

	Calculated VF value					
	from RNFL		from GCC		from GCL+IPL	
	R	*p*	*r*	*p*	*r*	*p*
Measured mean of threshold	**0.87**	**<0.001**	**0.78**	**<0.001**	**0.63**	**<0.001**
Measured mean of TD	**0.86**	**<0.001**	**0.77**	**<0.001**	**0.62**	**<0.001**
Measured mean of PD	**0.64**	**<0.001**	0.35	0.07	0.22	0.25

Values in bold are statistically significant.

capillaries. Additionally, automatic segmentation of the retinal layers becomes difficult when the layers are very thin. In the nasal area, these factors combine to lower the value of the correlation coefficient between macular structure and function.

We used the inverse calculation with the correlation formula between RNFLT and the threshold to create simulated visual fields, and found that they were significantly correlated with real visual fields. Since it is important to assess the relationship between structure and function to adequately diagnose and manage glaucoma, visual field examinations must be included in routine tests for patients with visual field loss. In certain situations, however, speculation based on visual field simulations created from macular OCT maps may be worthwhile. In routine visual field tests, the HFA 24-2 or 30-2 programs are used more often than 10-2. It is usually inconvenient to perform examinations with the both 24-2 or 30-2 and 10-2 programs on the same day, due to the length of time required and the fatigue imposed on the patient. Visual field simulations may be especially helpful in examining patients with mental deterioration or dementia.

We acknowledge the limitations of this study. First, it comprised only a small number of glaucoma patients, and the nature of the study was retrospective. Second, the correlation between structure and function has been reported to be biased by age, axial length, stage of glaucoma and myopia.[15,16] To decrease the influence of these biases on the results, we excluded from the study patients with relatively high myopia (less than −8 diopter) and glaucoma, and used a single regression analysis to confirm that the spherical equivalent was not associated with any of the macular OCT map parameters from this study (Table 2). Third, although there was anatomical displacement of the RNFL,[17] GCC,[10] and GCL + IPL[18] in the fovea, we did not include it in our assessment of the structure and function relationship. Finally, assessment of the macula in glaucoma patients has a built-in selection bias, because in most cases, patients examined with the 10-2 HFA tend to have evidence of glaucomatous damage in the macula. The macula, however, is not always involved in the progress of glaucoma. In the future, a larger, multicenter study may be necessary.

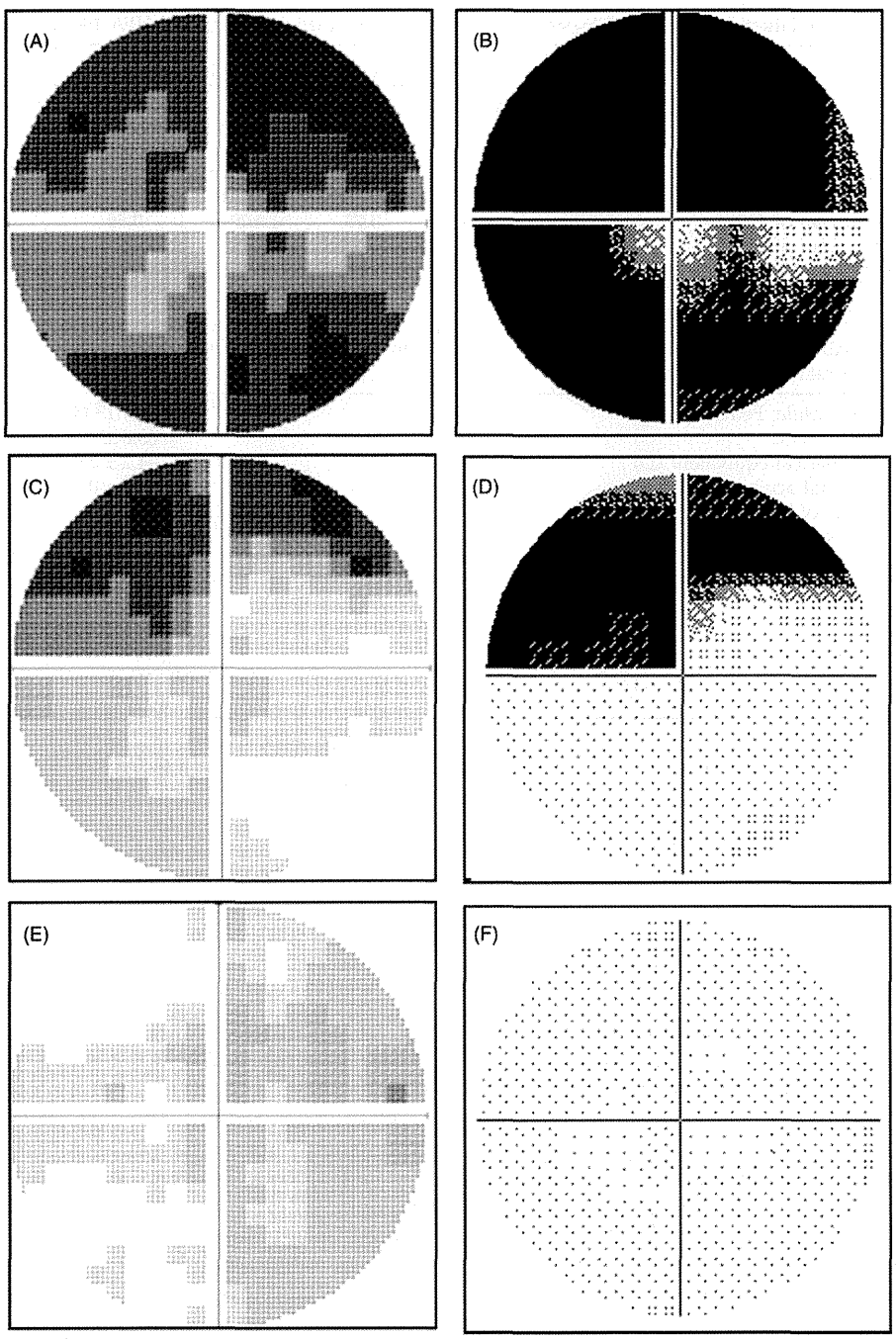

FIGURE 3 Comparison between simulated grayscale maps and real HFA 10-2 results of in three cases of glaucoma. The grayscale maps show the simulated visual field (VF) (A, C, E) and real VF (B, D, F). (A, B) Case 1. (C, D) Case 2. (E, F) Case 3.

In conclusion, we found that there were significant correlation between structure and function in the macular area, which enabled us to create simulated visual fields from RNFLT data with a high degree of similarity to actual visual fields. Such a simulation of macular function, derived from OCT parameters, may be of help in assessments of glaucoma, particularly in assessments of patients who have difficulty undergoing actual visual field examinations.

DECLARATION OF INTEREST

The authors report no conflict of interest.

REFERENCES

1. Quigley HA. Number of people with glaucoma worldwide. Br J Ophthalmol 1996;80:389–393.
2. Quigley HA, Broman AT. The number of people with glaucoma worldwide in 2010 and 2020. Br J Ophthalmol 2006;90:262–267.
3. Quigley HA, Dunkelberger GR, Green WR. Retinal ganglion cell atrophy correlated with automated perimetry in human eyes with glaucoma. Am J Ophthalmol 1989;107: 453–464.
4. Huang D, Swanson EA, Lin CP, Schuman JS, Stinson WG, Chang W, et al. Optical coherence tomography. Science 1991;254:1178–1181.
5. Guedes V, Schuman JS, Hertzmark E, Wollstein G, Correnti A, Mancini R, et al. Optical coherence tomography measurement of macular and nerve fiber layer thickness in normal and glaucomatous human eyes. Ophthalmology 2003;110:177–189.
6. Greenfield DS, Bagga H, Knighton RW. Macular thickness changes in glaucomatous optic neuropathy detected using optical coherence tomography. Arch Ophthalmol 2003;121: 41–46.
7. Lederer DE, Schuman JS, Hertzmark E, Heltzer J, Velazques LJ, Fujimoto JG, et al. Analysis of macular volume in normal and glaucomatous eyes using optical coherence tomography. Am J Ophthalmol 2003;135: 838–843.
8. Wollstein G, Schuman JS, Price LL, Aydin A, Beaton SA, Stark PC, et al. Optical coherence tomography (OCT) macular and peripapillary retinal nerve fiber layer measurements and automated visual fields. Am J Ophthalmol 2004;138:218–225.
9. Mwanza JC, Oakley JD, Budenz DL, Chang RT, Knight OJ, Feuer WJ. Macular ganglion cell-inner plexiform layer: automated detection and thickness reproducibility with spectral domain-optical coherence tomography in glaucoma. Invest Ophthalmol Vis Sci 2011;52:8323–8329.
10. Kim NR, Lee ES, Seong GJ, Kim JH, An HG, Kim CY. Structure-function relationship and diagnostic value of macular ganglion cell complex measurement using Fourier-domain OCT in glaucoma. Invest Ophthalmol Vis Sci 2010;51:4646–4651.
11. Seong M, Sung KR, Choi EH, Kang SY, Cho JW, Um TW, et al. Macular and peripapillary retinal nerve fiber layer measurements by spectral domain optical coherence tomography in normal-tension glaucoma. Invest Ophthalmol Vis Sci 2010;51:1446–1452.
12. Omodaka K, Nakazawa T, Yokoyama Y, Doi H, Fuse N, Nishida K. Correlation between peripapillary macular fiber layer thickness and visual acuity in patients with open-angle glaucoma. Clin Ophthalmol 2010;4:629–635.
13. Anderson DR, Patella VM. Automated static perimetry. 2nd ed. St. Louis: Mosby; 1999.
14. Pavlidis M, Stupp T, Naskar R, Cengiz C, Thanos S. Retinal ganglion cells resistant to advanced glaucoma: a postmortem study of human retinas with the carbocyanine dye DiI. Invest Ophthalmol Vis Sci 2003;44: 5196–5205.
15. Kang SH, Hong SW, Im SK, Lee SH, Ahn MD. Effect of myopia on the thickness of the retinal nerve fiber layer measured by Cirrus HD optical coherence tomography. Invest Ophthalmol Vis Sci 2010;51:4075–4083.
16. Leung CK, Yu M, Weinreb RN, Ye C, Liu S, Lai G, et al. Retinal nerve fiber layer imaging with spectral-domain optical coherence tomography: a prospective analysis of age-related loss. Ophthalmology 2012;119: 731–737.
17. Drasdo N, Millican CL, Katholi CR, Curcio CA. The length of Henle fibers in the human retina and a model of ganglion receptive field density in the visual field. Vision Res 2007;47:2901–2911.
18. Raza AS, Cho J, de Moraes CG, Wang M, Zhang X, Kardon RH, et al. Retinal ganglion cell layer thickness and local visual field sensitivity in glaucoma. Arch Ophthalmol 2011; 129:1529–1536.

Experimental Eye Research 108 (2013) 10–15

Contents lists available at SciVerse ScienceDirect

Experimental Eye Research

journal homepage: www.elsevier.com/locate/yexer

Comparison of CCD-equipped laser speckle flowgraphy with hydrogen gas clearance method in the measurement of optic nerve head microcirculation in rabbits

Hiroaki Takahashi [a], Tetsuya Sugiyama [b,*], Hideki Tokushige [a], Takatoshi Maeno [c], Toru Nakazawa [d], Tsunehiko Ikeda [b], Makoto Araie [e]

[a] Research Laboratory for Drug Development, Senju Pharmaceutical Co., Ltd., 1-5-4 Murotani, Nishi-ku, Kobe, Hyogo 651-2241, Japan
[b] Department of Ophthalmology, Osaka Medical College, 2-7 Daigaku-machi, Takatsuki, Osaka 569-8686, Japan
[c] Department of Ophthalmology, Toho University Sakura Medical Center, 564-1 Shimoshizu, Sakura, Chiba 285-8741, Japan
[d] Department of Ophthalmology, Tohoku University Graduate School of Medicine, 1-1 Seiryo-machi, Aoba-ku, Sendai, Miyagi 980-8574, Japan
[e] Kanto Central Hospital of The Mutual Aid Association of Public School Teachers, 6-25-1 Kamiyoga, Setagaya-ku, Tokyo 158-0098, Japan

ARTICLE INFO

Article history:
Received 6 October 2012
Accepted in revised form 10 December 2012
Available online 19 December 2012

Keywords:
optic nerve head
laser speckle flowgraphy
mean blur rate
hydrogen gas clearance method
capillary blood flow
rabbit

ABSTRACT

The aim of this study was to verify the correlation between mean blur rate (MBR) obtained with CCD-equipped laser speckle flowgraphy (LSFG) and capillary blood flow (CBF) obtained by the hydrogen gas clearance method in rabbit optic nerve head (ONH). Using Japanese white rabbits under systemic anesthesia, a hydrogen electrode was inserted an area of the ONH free from superficial capillaries. MBR was measured with LSFG near the hydrogen electrode. CBF and MBR were measured in the range of 32.4–83.5 mL/min/100 g and 3.5–6.0, respectively. MBR and CBF were significantly correlated ($r = 0.73$, $P < 0.01$, $n = 14$). After inhalation of carbon dioxide (CO_2) or intravenous administration of endothelin-1 (ET-1), MBR and CBF were changed in the relative range of 0.74–1.27 and 0.76–1.35, respectively. The relative changes in MBR and CBF induced by CO_2 and ET-1 were also significantly correlated ($r = 0.67$, $P < 0.01$). The current results suggest that MBR may correlate with CBF and also change with CBF, as an index of blood flow in the ONH, linearly.

1. Introduction

Abnormal blood flow regulation is widely recognized to contribute to the pathophysiology of ocular diseases such as glaucoma (Grieshaber et al., 2007; Moore et al., 2008; Pemp et al., 2009). Circulatory factors in the retrobulbar arteries may be associated with the progression of visual field defects in patients with normal-tension glaucoma (Yamazaki and Drance, 1997). Progressive structural changes in the optic nerve head (ONH) also have been related to abnormal ocular blood flow in glaucoma patients (Harris et al., 2008b). For example, Logan et al. (2004) found lower levels of retinal blood flow in abnormal segments of the ONH than in a corresponding normal segment in glaucoma patients. In addition, glaucoma patients with normal rim segments demonstrated lower retinal blood flow than controls at each location sampled. However, the role played by blood flow and ischemia on the ONH and retina in glaucoma has not yet been clarified, in part because technical difficulties have limited the accurate measurement of ocular blood flow in relevant vascular beds (Caprioli and Coleman, 2010; Harris et al., 2008a).

The Association for Ocular Circulation (http://www.obfra.org/) has published consensus reports on ocular circulation measurement methods such as laser Doppler flowmetry (Riva et al., 2010), laser speckle flowgraphy (LSFG) (Sugiyama et al., 2010), retinal vessel analysis (Garhofer et al., 2010), and color Doppler imaging (Stalmans et al., 2011). Among them, LSFG is the only method available to measure tissue circulation non-invasively and provide a 2-dimensional map of ocular tissue circulation. Normalized blur (NB) was the value used previously in LSFG and represents an index of blood velocity (Tamaki et al., 1994, 1995). *In vitro*, NB demonstrated a good linear correlation with the mean velocity of blood cells flowing through a glass capillary tube (calculated from the blood flow rate generated by a calibrated peristaltic pump) (Nagahara et al., 1999) and with the speed of rotation of a ground-

Abbreviations: CBF, capillary blood flow; LSFG, laser speckle flowgraphy; MBR, mean blur rate; ONH, optic nerve head.

* Corresponding author. Tel.: +81 72 683 1221; fax: +81 72 681 8195.
E-mail addresses: tsugiyama@poh.osaka-med.ac.jp, tsugiyama7@gmail.com (T. Sugiyama).

0014-4835/$ – see front matter © 2012 Elsevier Ltd. All rights reserved.
http://dx.doi.org/10.1016/j.exer.2012.12.003

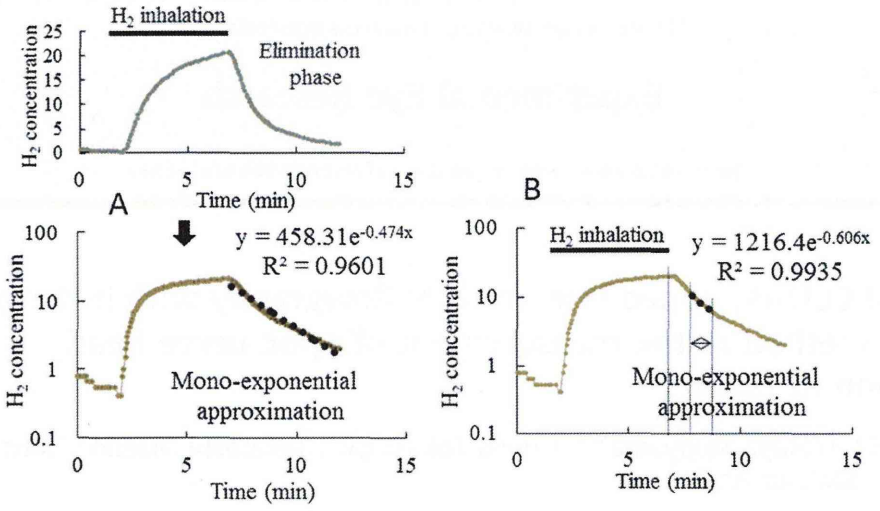

Fig. 1. An example of analyzing hydrogen clearance curve to obtain capillary blood flow (CBF) by the hydrogen gas clearance method. The hydrogen concentration was plotted into logarithm (A). The half-life ($T_{1/2}$) at 1–2 min after stopping hydrogen inhalation was adopted for calculation because the linearity of hydrogen clearance in logarithm was the highest there (B). We then calculate CBF as $69.3/T_{1/2}$ (ml/min/100 g).

glass disc (calculated from the velocity of diffusing particles, which are models of blood cells, on the glass) (Nagahara et al., 1999; Tamaki et al., 1994, 1995,). *In vivo*, NB was well correlated with tissue blood flow rates determined using the microsphere method in the retina, choroid, or iris, as well as blood flow rates determined with the hydrogen gas clearance method in the ONH (Sugiyama et al., 1996; Takayama et al., 2003; Tamaki et al., 1994, 1995, 1996, 2003; Tomidokoro et al., 1998; Tomita et al., 1999).

In 2008, LSFG-NAVI™ was approved as a medical apparatus by the Pharmaceuticals and Medical Devices Agency in Japan. It has adopted a new index: mean blur rate (MBR), the relative velocity index of erythrocytes (Konishi et al., 2002; Watanabe et al., 2008). Recently, Aizawa et al. (2011) reported that MBR has high reproducibility in normal and glaucoma subjects. However, no reports to date have investigated whether MBR is correlated with blood flow rate in the ONH.

The hydrogen gas clearance technique provides multiple capillary blood flow (CBF) measurements quantitatively over long periods of time (Aukland et al., 1964; Csete et al., 2004; Srinivasan et al., 2011). In the ophthalmic field, this technique has been applied to the ONH in rhesus monkeys (Ernest, 1976) and demonstrated high reproducibility in the measurement of CBF in rabbit ONH (Sugiyama et al., 1995). However, use of this technique is limited to laboratory research because it is highly invasive. The aim of the current study was to verify the correlation between MBR obtained by LSFG and CBF obtained by the hydrogen gas clearance method in the rabbit ONH.

2. Materials and methods

2.1. Animals

Eighteen male Japanese white rabbits weighing 2.5–3.3 kg were purchased from Kitayama Lab. (Nagano, Japan) for the current study. They were housed in an air-conditioned room at temperature of 23 ± 3 °C and humidity of 55 ± 10% with a 12-h light–dark cycle and provided with tap water *ad libitum* throughout the experimental period. All animal studies were performed in accordance with the ARVO statement for the use of animals in ophthalmic and vision research and with the approval of the Institutional Animal Care and Use Committee of Kobe Creative Center, Senju Pharmaceutical Co., Ltd.

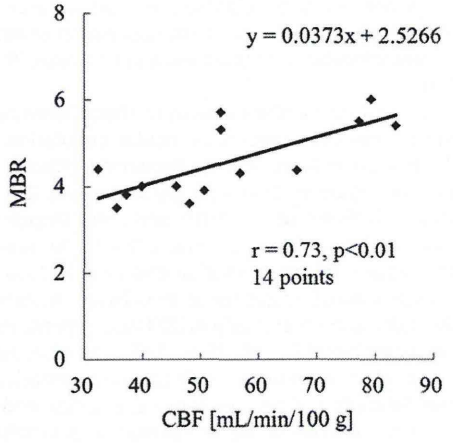

Fig. 2. Correlation between the absolute values of CBF and MBR at baseline. CBF and MBR were obtained by the hydrogen gas clearance method and LSFG, respectively. Each point represents 1 of 14 different rabbits. Correlation coefficient (r) was 0.73 ($P < 0.01$).

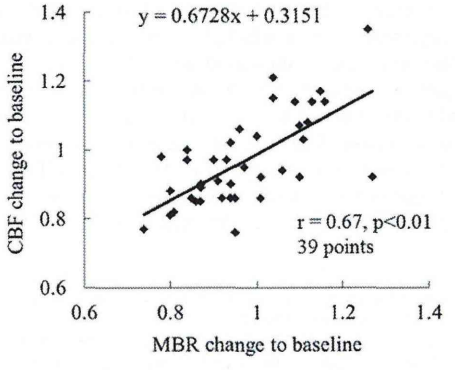

Fig. 3. Correlation between the relative changes in CBF and MBR after treatment with CO_2 and ET-1. Each point represents the ratio of relative values to baseline values. Total points were obtained from 39 time points ($n = 9$ and 6 for CO_2 and ET-1, respectively) in 10 eyes of 14 rabbits. Correlation coefficient (r) was 0.67 ($P < 0.01$).

Table 1
Distributions of variances by randomized block ANOVA regarding individuality and time-course changes after each treatment.

Treatment	Individuality		Time-course changes	
	CBF	MBR	CBF	MBR
CO_2	569.268 (8)*	15.046 (8)*	68.750 (3)*	1.358 (3)*
ET-1	262.346 (5)*	1.834 (5)*	11.056 (2)	0.127 (2)

Asterisks represent significant differences ($P < 0.05$) among values obtained from individual rabbits or values at different time points. Degrees of freedom were shown in parentheses.

2.2. Measurement of CBF in ONH

Mydriasis was induced by topical tropicamide (Mydrin®-M ophthalmic solution 0.4%, Santen Pharmaceutical Co. Ltd., Osaka, Japan). Animals were anesthetized by intraperitoneal injection of 0.8 mg/kg urethane at 0.4 g/mL (Nakalai, Kyoto, Japan) and additional intramuscular injection of 0.1 mg/kg urethane as necessary. Topical anesthesia was induced by topical oxybuprocaine (Benoxil® ophthalmic solution 0.4%, Santen Pharmaceutical Co. Ltd.). The CBF in the ONH was measured by the hydrogen gas clearance method as previously reported (Sugiyama et al., 1996). A hydrogen electrode (Cat.# OA211-013, platinum needle with a 0.7-mm long and 0.1-mm diameter Pt—Ir tip, Unique Medical Co., Ltd., Tokyo, Japan) was inserted into a lower portion of the ONH with no visible surface vessels through the vitreous body from the pars plana using a vitrectomy lens. The reference electrode was subcutaneously fixed on the head. After the inhalation of 10% hydrogen gas by a mask at 5 L/min for 5 min, CBF was calculated with the hydrogen concentration half-life ($T_{1/2}$) using a hydrogen clearance flow meter (model MDH-D1, Unique Medical Co., Ltd.). As shown in Fig. 1A, since the clearance curve is approximately mono-exponential, the hydrogen concentration was plotted into logarithm to get half-life ($T_{1/2}$) for calculation. Specifically in the current study, the linearity of hydrogen clearance in logarithm was found beforehand to be the highest at 1–2 min after stopping hydrogen inhalation (Fig. 1B), therefore we adopted the half-life there to calculate CBF as $69.3/T_{1/2}$ (mL/min/100 g).

2.3. Measurement method of MBR in ONH

MBR was measured with a LSFG-NAVI-MRC™ device (Softcare Ltd., Iizuka, Japan). The LSFG-NAVI-MRC™ consisted of a fundus camera equipped with a diode laser (wavelength: 830 nm) and a CCD image sensor (750 × 360 pixels). The principle and application of this method have been described previously (Konishi et al., 2002; Sugiyama et al., 2010; Tamaki et al., 1995). The measurement area of MBR was designated as a square area free of visible surface vessels near the hydrogen electrode in the ONH.

2.4. Measurements of CBF and MBR before and after altering ONH blood flow

To check their stability in measuring ONH blood flow, CBF and MBR were recorded 3 times at 15-min intervals and 5 times at 5-min intervals, respectively. The intervals were recommended in previous reports (Sugiyama and Azuma, 1995; Tamaki et al., 1995). The inclusion criterion for the stability of measurements was a coefficient of variance (CV) of CBF within 0.1. Averages of measurement values were adopted as baseline values. The correlation between the baseline values of CBF and MBR was estimated. Baseline values were measured before the inhalation of carbon dioxide (CO_2) or intravenous administration of endothelin-1 (ET-1).

Immediately, 15, and 30 min after 5-min inhalation of 10% CO_2 in ordinary air via mask at 5 L/min, CBF and MBR were measured simultaneously in the same rabbit. CBF was measured once at each time point. MBR was recorded 5 times at each time point, and then the mean value was calculated. Human ET-1 (Peptide Institute, Osaka, Japan) was dissolved in 0.1% aqueous acetic acid to provide a 10^{-4} mol/L concentration and diluted with saline for a 10^{-6} mol/L solution. CBF and MBR were measured, as above, at 30 min and 1 h after intravenous injection (10^{-10} mol/kg) of the prepared ET-1 solution. The relative change in CBF and MBR was calculated by dividing by the baseline value. The expiratory CO_2 density and arterial O_2 and CO_2 pressure were not monitored.

2.5. Statistical analysis

Correlation analysis between CBF and MBR was performed using Ekuseru-Toukei 2008 statistical software (Social Survey Research Information Co., Ltd., Tokyo, Japan). We analyzed the effects of each treatment (namely, CO_2 and ET-1) on MBR and CBF by randomized block ANOVA with individual animals as a block using JMP software (Ver. 9.0.0, SAS Institute, Cary, NC). Findings of $P < 0.05$ were considered significant.

3. Results

3.1. Correlation between the baseline values of CBF and MBR

A plot of baseline CBF and MBR values is shown in Fig. 2. In 17 of 18 rabbits, the CV of CBF was within 0.1. For measurement of MBR in 3 of 17 rabbits, the square area could not be designated free from visible surface vessels near the hydrogen electrode in the ONH. Therefore, data from 14 eyes of 14 rabbits were used for this analysis. CBF and MBR were measured in the range (mean ± SE) of 32.4–83.5 (54.3 ± 4.5) mL/min/100 g and 3.5–6.0 (4.6 ± 0.2), respectively. A significant positive correlation between the absolute CBF and MBR baseline values was observed ($r = 0.73$, $P < 0.01$, $n = 14$).

3.2. Correlation between the relative change in CBF and MBR induced by inhalation of CO_2 and intravenous administration of ET-1

CBF was altered after inhalation of CO_2 or intravenous administration of ET-1. Relative values of CBF changed in the range of 0.74–1.27. MBR in the ONH was also altered. Relative values of MBR changed in the range of 0.76–1.35. A plot of relative changes in CBF and MBR is shown in Fig. 3. In 10 of 14 rabbits, the changes in CBF and MBR induced by CO_2 ($n = 9$) and ET-1 ($n = 6$) were measured with the hydrogen gas clearance method and LSFG, respectively. The relative changes in CBF and MBR demonstrated a significant positive correlation ($r = 0.67$, $P < 0.01$).

Table 2
Average changes in CBF and MBR after inhalation of CO_2.

	Baseline levels	Immediately	15 min	30 min
CBF (mL/min/100 g)	50.7 ± 11.5	52.3 ± 12.1 (1.04 ± 0.11)	48.3 ± 14.2 (0.95 ± 0.14)	46.0 ± 11.4* (0.91 ± 0.10)
MBR	4.7 ± 2.0	5.0 ± 2.0* (1.08 ± 0.10)	4.6 ± 2.5 (0.97 ± 0.13)	4.0 ± 1.4* (0.89 ± 0.08)

Data are expressed as mean ± SD for 9 rabbits. Asterisks represent significant differences ($P < 0.05$) compared to baseline levels by paired t-test. CBF/MBR changes to baseline levels were shown in parentheses.

Table 3
Average changes in CBF and MBR after intravenous administration of ET-1.

	Baseline levels	30 min	60 min
CBF (mL/min/100 g)	41.6 ± 10.2	41.9 ± 9.8 (1.02 ± 0.15)	39.4 ± 10.5 (0.95 ± 0.16)
MBR	4.1 ± 0.8	3.9 ± 1.0 (0.95 ± 0.08)	3.9 ± 0.7 (0.95 ± 0.20)

Data are expressed as mean ± SD for 6 rabbits. No significant difference was found. CBF/MBR changes to baseline levels were shown in parentheses.

3.3. *Effects of individuality and treatment*

Randomized block ANOVA revealed that there were wide ranges of distribution of differences for the basal blood flow measurement and that animals' individuality had significant effects on MBR and CBF (Table 1). Distributions of differences for the time-course changes were relatively narrow. Although the time-course changes in MBR and CBF during ET-1 treatment were not significant, those during CO_2 treatment were significant by repeated measure analysis (Table 1).

Average and individual changes in CBF after treatments are shown in Tables 2 and 3 and Fig. 4, respectively. CBF had a tendency of increasing after CO_2 inhalation (CBF was increased in 6 cases out of 9). ET-1 administration decreased CBF in 5 cases out of 6 though the effect was not significant because CBF was markedly increased in just one case. Representative hydrogen density curve charts are shown in Fig. 5. Average changes in MBR after treatments are shown in Tables 2 and 3. Typical examples of 2-dimensional color-coded MBR maps are shown in Fig. 6.

4. Discussion

This report is the first to verify the correlation of MBR, a new index obtained by CCD-equipped LSFG, with CBF obtained by the hydrogen gas clearance method in the ONH. A significant and positive correlation between the absolute values of CBF and MBR at baseline, as well as their relative changes, was found in the current study. This result suggests that MBR may correlate with CBF and also change with CBF, as an index of blood flow in the ONH, linearly. Since a similar experiment cannot be performed in humans, the present study provides important basal data for the measurement of MBR in humans, though these data cannot be applied directly to humans because of their many histophysiological differences with rabbits.

A power analysis (Correlation: point biserial model) by G* Power software (v. 3.1.3) showed that total sample size of 9 is needed under the condition of effect size of 0.7, error probability (α) of 0.05 and power ($1 - \beta$) of 0.8. Therefore, the sample sizes of 14 and 39 in the current study would be sufficient statistically.

In the present study, inhalation of CO_2 or intravenous administration of ET-1 altered CBF obtained by the hydrogen gas clearance method in rabbit ONH. These results are, at least partly, consistent with previous reports (Sugiyama et al., 1995, 1996). The relative values of CBF and MBR to the initial levels were in the range of 0.74–1.27 and 0.76–1.35, respectively. A significant and positive correlation was also found between the relative changes in CBF and MBR values induced by CO_2 inhalation and ET-1 injection. This correlation suggests that changes in MBR may indicate those in CBF in the ONH. These results appear similar to a previous report (Sugiyama et al., 1996). Though the r value in this study (0.67) was obviously different from that in the previous paper (0.92), the comparison of r values from different experiments does not seem fair since they can be affected by many factors.

In the current study, the r value for the correlation between the absolute values of MBR and CBF was 0.73; this was relatively large and comparable to that between the relative values during CO_2 inhalation and ET-1 injection. This result indicates quantifiability of absolute values of MBR at least under a certain condition. On the other hand, the randomized block ANOVA in the current study revealed significant effects of the individuality of animals on basal values of CBF and MBR. Therefore, care must be taken in interpreting absolute values across individuals, even though the absolute values of MBR were significantly correlated with CBF. In general, measurement results obtained with apparatus that employ lasers are affected by the degree of absorption or reflection of the laser beam in the specific tissue. Particularly in humans, careful interpretation is needed due to relatively large topographical or color differences of the ONH induced by individuality or diseases, which affect absorption and reflection. Actually, we have data on individual variation in MBRs of young normal volunteers; MBRs in the temporal rim were measured in the range of 6.3–13.8 (mean ± SD = 10.6 ± 2.5, n = 9). In addition, MBRs in the nasal

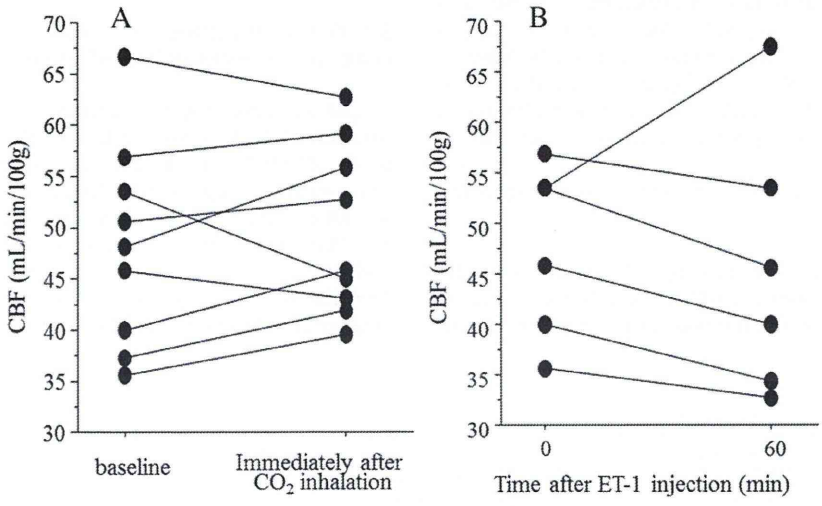

Fig. 4. Individual changes in CBF after 5-min inhalation of 10% CO_2 (A) and administration of 10^{-10} mol/kg ET-1 (B). CBF was increased in 6 cases out of 9, and decreased in 5 cases out of 6 in A and B, respectively.

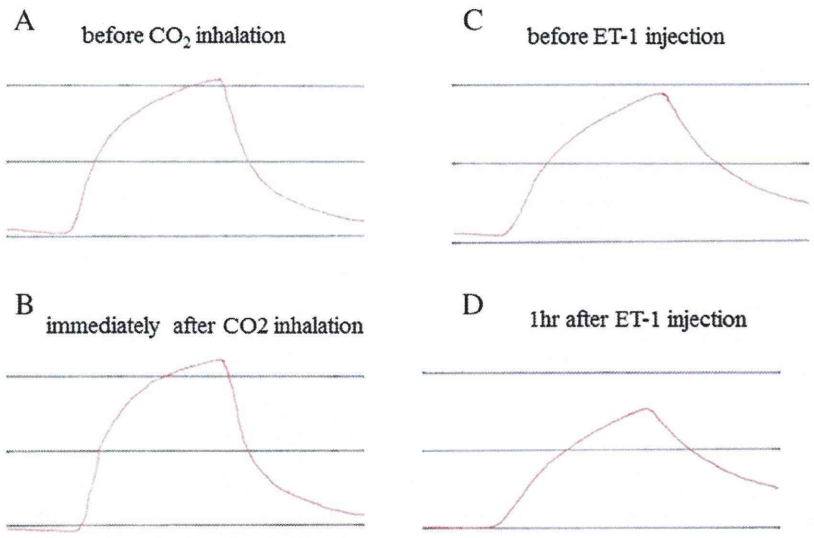

Fig. 5. Representative examples of the hydrogen gas clearance curve. A and B: before and immediately after 5-min inhalation of 10% CO_2 in the same rabbit (A is the same as Fig. 1A). CBF values were 65.3 and 77.6 mL/min/100 g, respectively. C and D: before and 1 h after administration of 10^{-10} mol/kg ET-1 in another same rabbit. CBF values were 40.3 and 32.8 mL/min/100 g, respectively.

rim of them were measured as 17.8 ± 3.9, which are much different from those in the temporal rim. Therefore, the relatively wide range of ONH blood flow in the present study might be due to an individual difference as well as a regional difference.

As a problematic issue for the LSFG apparatus, the zero-offset for MBR was rather large (around 2.5) in the current study. We actually obtained 6.1 and 1.9 as mean values of MBR ($n = 2$) at the same spot of ONH just before and shortly after a rabbit was euthanized (the hydrogen gas clearance method cannot be available while it is dead because inhalation is impossible then) in the additional experiment. This result (mean value of MBR was 1.9 when blood flow was stopped in dead rabbits) is almost consistent with the zero-offset of approximately 2.5. In addition, since a range of baseline values of MBR was 3.5–6.0, the ratio of the highest to the lowest (6.0/3.5) was smaller than those by the hydrogen gas clearance method (83.5/32.4). Taken together, there seems to be a room for more

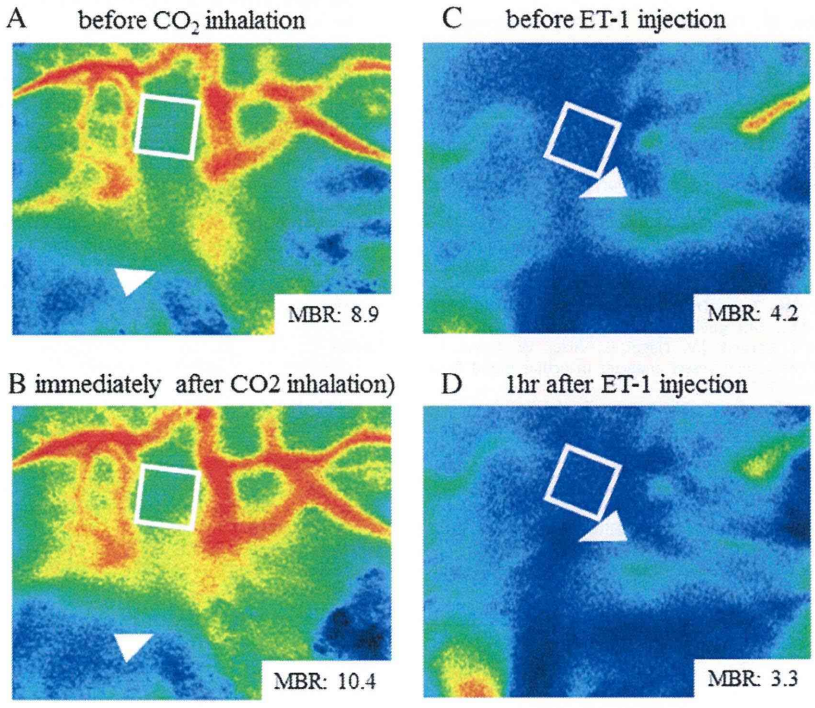

Fig. 6. Representative examples of color-coded MBR maps obtained by LSFG. A and B: before and immediately after 5-min inhalation of 10% CO_2 in the same rabbit. C and D: before and 1 h after administration of 10^{-10} mol/kg ET-1 in another rabbit. Arrowheads indicate the tips of electrodes for the hydrogen gas clearance method, and white squares indicate the areas analyzed by LSFG.

adequate calibration of MBR values. While these results (a relatively large zero-offset and a smaller relative change in MBR) were only for the animal model in the current study. Further investigation using other animals should also be needed in the future for validation of quantifiability of measurement of ONH microcirculation by LSFG.

Many agents have been reported to alter ocular blood flow (Araie and Mayama, 2011; Shimazawa et al., 1999; Sugiyama and Azuma, 1995; Sugiyama et al., 2010, 2011; Tokushige et al., 2011; Waki et al., 2001). Since the present study revealed that MBR may correlate with tissue blood flow in the ONH, LSFG-NAVI™ will likely provide new relevant information concerning the ONH blood flow in glaucoma and support in verifying whether increasing ONH blood flow could be a promising strategy for glaucoma management.

5. Conclusions

Our results suggest that MBR obtained by CCD-equipped LSFG may correlate with CBF and also change with CBF, as an index of blood flow in the ONH, linearly.

Financial disclosure

H. Takahashi and H. Tokushige are employees of Senju Pharmaceutical Co., Ltd. The other authors have no financial disclosures.

Acknowledgments

The authors thank Y.T. for her technical support and kindest encouragement, Mr. Mitsunori Waki for his technical advice and valuable discussions, and Dr. Tomoyuki Wada for his advice concerning statistics and his encouragement.

References

Aizawa, N., Yokoyama, Y., Chiba, N., Omodaka, K., Yasuda, M., Otomo, T., Nakamura, M., Fuse, N., Nakazawa, T., 2011. Reproducibility of retinal circulation measurements obtained using laser speckle flowgraphy-NAVI in patients with glaucoma. Clin. Ophthalmol. 5, 1171–1176.

Araie, M., Mayama, C., 2011. Use of calcium channel blockers for glaucoma. Prog. Retin. Eye Res. 30, 54–71.

Aukland, K., Bower, B.F., Berliner, R.W., 1964. Measurement of local blood flow with hydrogen gas. Circ. Res. 14, 164–187.

Caprioli, J., Coleman, A.L., 2010. Blood pressure, perfusion pressure, and glaucoma. Am. J. Ophthalmol. 149, 704–712.

Csete, K., Vezekényi, Z., Dóczi, T., Papp, J.G., Bodosi, M., Barzó, P., 2004. Comparison of regional vasomotor responses to acetazolamide and CO_2 in rabbit cerebrum and cerebellum, measured by a hydrogen clearance method. Acta Physiol. Scand. 182, 287–294.

Ernest, J.T., 1976. Optic disc blood flow. Trans. Ophthalmol. Soc. U.K. 96, 348–351.

Garhofer, G., Bek, T., Boehm, A.G., Gherghel, D., Grunwald, J., Jeppesen, P., Kergoat, H., Kotliar, K., Lanzl, I., Lovasik, J.V., Nagel, E., Vilser, W., Orgul, S., Schmetterer, L., 2010. Use of the retinal vessel analyzer in ocular blood flow research. Acta Ophthalmol. 88, 717–722.

Grieshaber, M.C., Mozaffarieh, M., Flammer, J., 2007. What is the link between vascular dysregulation and glaucoma? Surv. Ophthalmol. 52 (Suppl. 2), S144–S154.

Harris, A., Kagemann, L., Ehrlich, R., Rospigliosi, C., Moore, D., Siesky, B., 2008a. Measuring and interpreting ocular blood flow and metabolism in glaucoma. Can. J. Ophthalmol. 43, 328–336.

Harris, A., Werne, A., Cantor, L.B., 2008b. Vascular abnormalities in glaucoma: from population-based studies to the clinic? Am. J. Ophthalmol. 145, 595–597.

Konishi, N., Tokimoto, Y., Kohra, K., Fujii, H., 2002. New laser speckle flowgraphy system using CCD camera. Opt. Rev. 9, 163–169.

Logan, J.F., Rankin, S.J., Jackson, A.J., 2004. Retinal blood flow measurements and neuroretinal rim damage in glaucoma. Br. J. Ophthalmol. 88, 1049–1054.

Moore, D., Harris, A., Wudunn, D., Kheradiya, N., Siesky, B., 2008. Dysfunctional regulation of ocular blood flow: a risk factor for glaucoma? Clin. Ophthalmol. 2, 849–861.

Nagahara, M., Tamaki, Y., Araie, M., Fujii, H., 1999. Real-time blood velocity measurements in human retinal vein using the laser speckle phenomenon. Jpn. J. Ophthalmol. 43, 186–195.

Pemp, B., Georgopoulos, M., Vass, C., Fuchsjager-Mayrl, G., Luksch, A., Rainer, G., Schmetterer, L., 2009. Diurnal fluctuation of ocular blood flow parameters in patients with primary open-angle glaucoma and healthy subjects. Br. J. Ophthalmol. 93, 486–491.

Riva, C.E., Geiser, M., Petrig, B.L., 2010. Ocular blood flow assessment using continuous laser doppler flowmetry. Acta Ophthalmol. 88, 622–629.

Shimazawa, M., Sugiyama, T., Azuma, I., Araie, M., Iwakura, Y., Watari, M., Sakai, T., Hara, H., 1999. Effect of lomerizine, a new Ca^{2+}channel blocker, on the microcirculation in the optic nerve head in conscious rabbits: a study using a laser speckle technique. Exp. Eye Res. 69, 185–193.

Srinivasan, V.J., Atochin, D.N., Radhakrishnan, H., Jiang, J.Y., Ruvinskaya, S., Wu, W., Barry, S., Cable, A.E., Ayata, C., Huang, P.L., Boas, D.A., 2011. Optical coherence tomography for the quantitative study of cerebrovascular physiology. J. Cereb. Blood Flow Metab. 31, 1339–1345.

Stalmans, I., Vandewalle, E., Anderson, D.R., Costa, V.P., Frenkel, R.E., Garhofer, G., Grunwald, J., Gugleta, K., Harris, A., Hudson, C., Januleviciene, I., Kagemann, L., Kergoat, H., Lovasik, J.V., Lanzl, I., Martinez, A., Nguyen, Q.D., Plange, N., Reitsamer, H.A., Sehi, M., Siesky, B., Zeitz, O., Orgul, S., Schmetterer, L., 2011. Use of colour doppler imaging in ocular blood flow research. Acta Ophthalmol. 89, e609–630.

Sugiyama, T., Araie, M., Riva, C.E., Schmetterer, L., Orgul, S., 2010. Use of laser speckle flowgraphy in ocular blood flow research. Acta Ophthalmol. 88, 723–729.

Sugiyama, T., Azuma, I., 1995. Effect of UF-021 on optic nerve head circulation in rabbits. Jpn. J. Ophthalmol. 39, 124–129.

Sugiyama, T., Moriya, S., Oku, H., Azuma, I., 1995. Association of endothelin-1 with normal tension glaucoma: clinical and fundamental studies. Surv. Ophthalmol. 39 (Suppl. 1), S49–S56.

Sugiyama, T., Shibata, M., Kajiura, S., Okuno, T., Tonari, M., Oku, H., Ikeda, T., 2011. Effects of fasudil, a rho-associated protein kinase inhibitor, on optic nerve head blood flow in rabbits. Invest. Ophthalmol. Vis. Sci. 52, 64–69.

Sugiyama, T., Utsumi, T., Azuma, I., Fujii, H., 1996. Measurement of optic nerve head circulation: comparison of laser speckle and hydrogen clearance methods. Jpn. J. Ophthalmol. 40, 339–343.

Takayama, J., Tomidokoro, A., Ishii, K., Tamaki, Y., Fukaya, Y., Hosokawa, T., Araie, M., 2003. Time course of the change in optic nerve head circulation after an acute increase in intraocular pressure. Invest. Ophthalmol. Vis. Sci. 44, 3977–3985.

Tamaki, Y., Araie, M., Fukaya, Y., Nagahara, M., Imamura, A., Honda, M., Obata, R., Tomita, K., 2003. Effects of lomerizine, a calcium channel antagonist, on retinal and optic nerve head circulation in rabbits and humans. Invest. Ophthalmol. Vis. Sci. 44, 4864–4871.

Tamaki, Y., Araie, M., Kawamoto, E., Eguchi, S., Fujii, H., 1995. Non-contact, two-dimensional measurement of tissue circulation in choroid and optic nerve head using laser speckle phenomenon. Exp. Eye Res. 60, 373–383.

Tamaki, Y., Araie, M., Kawamoto, E., Eguchi, S., Fujii, H., 1994. Noncontact, two-dimensional measurement of retinal microcirculation using laser speckle phenomenon. Invest. Ophthalmol. Vis. Sci. 35, 3825–3834.

Tamaki, Y., Araie, M., Tomita, K., Tomidokoro, A., 1996. Time change of nicardipine effect on choroidal circulation in rabbit eyes. Curr. Eye Res. 15, 543–548.

Tokushige, H., Waki, M., Takayama, Y., Tanihara, H., 2011. Effects of Y-39983, a selective rho-associated protein kinase inhibitor, on blood flow in optic nerve head in rabbits and axonal regeneration of retinal ganglion cells in rats. Curr. Eye Res. 36, 964–970.

Tomidokoro, A., Araie, M., Tamaki, Y., Tomita, K., 1998. In vivo measurement of iridial circulation using laser speckle phenomenon. Invest. Ophthalmol. Vis. Sci. 39, 364–371.

Tomita, K., Araie, M., Tamaki, Y., Nagahara, M., Sugiyama, T., 1999. Effects of nilvadipine, a calcium antagonist, on rabbit ocular circulation and optic nerve head circulation in NTG subjects. Invest. Ophthalmol. Vis. Sci. 40, 1144–1151.

Waki, M., Sugiyama, T., Watanabe, N., Ogawa, T., Shirahase, H., Azuma, I., 2001. Effect of topically applied iganidipine dihydrochloride, a novel calcium antagonist, on optic nerve head circulation in rabbits. Jpn. J. Ophthalmol. 45, 76–83.

Watanabe, G., Fujii, H., Kishi, S., 2008. Imaging of choroidal hemodynamics in eyes with polypoidal choroidal vasculopathy using laser speckle phenomenon. Jpn. J. Ophthalmol. 52, 175–181.

Yamazaki, Y., Drance, S.M., 1997. The relationship between progression of visual field defects and retrobulbar circulation in patients with glaucoma. Am. J. Ophthalmol. 124, 287–295.

Current Eye Research, 2013; 38(6): 691–698
© Informa Healthcare USA, Inc.
ISSN: 0271-3683 print / 1460-2202 online
DOI: 10.3109/02713683.2012.758292

informa
healthcare

ORIGINAL ARTICLE

The Influence of Posture Change on Ocular Blood Flow in Normal Subjects, Measured by Laser Speckle Flowgraphy

Yukihiro Shiga[1], Masahiko Shimura[2], Toshifumi Asano[1], Satoru Tsuda[1], Yu Yokoyama[1], Naoko Aizawa[1], Kazuko Omodaka[1], Morin Ryu[1], Shunji Yokokura[1], Takayuki Takeshita[1] and Toru Nakazawa[1]

[1]*Department of Ophthalmology, Tohoku University Graduate School of Medicine, Miyagi, Japan and* [2]*Department of Ophthalmology, NTT East Japan Tohoku Hospital, Sendai, Japan*

ABSTRACT

Purpose: To investigate, using laser speckle flowgraphy (LSFG), the autoregulation of ocular blood flow (BF) in response to posture change.

Methods: This study comprised 20 healthy volunteers (mean age 30.0 ± 8.5). The mean blur rate (MBR) of the ocular circulation in the subjects was assessed in both a sitting and a supine position every 2 min over the course of 10 min. Baseline measurements of the MBR at the optic nerve head (ONH) and the choroid were taken in a sitting position. Increases in the MBR ratio in a supine position were calculated with reference to this baseline. Intraocular pressure (IOP), systemic blood pressure and heart rate in the brachial artery were also recorded.

Results: In the ONH, the MBR ratio increased significantly over the baseline after 2 min ($104.8 \pm 5.0\%$, $p = 0.001$) and 4 min ($104.4 \pm 5.6\%$, $p = 0.005$), in a supine position, but decreased to the initial level after only 6 min. In the choroid, on the other hand, while the MBR ratio also increased significantly after 2 min in a supine position ($113.7 \pm 8.1\%$, $p < 0.001$), it kept this significant increase over the time course of 10 min. After 10 min in a supine position, IOP increased significantly ($p < 0.001$), systolic blood pressure decreased significantly ($p < 0.001$), but diastolic blood pressure did not change significantly compared to the baseline. ($p = 0.07$)

Conclusions: ONH and choroidal circulation have significantly different hemodynamics in response to posture change in healthy volunteers. This finding suggests that LSFG enables us to assess the autoregulation of BF in the ONH.

Keywords: Autoregulation, choroid, laser speckle flowgraphy, ocular blood flow, optic nerve head

INTRODUCTION

The regulation of blood flow (BF) in response to posture change is important to ensure an adequate supply of oxygen and nutrients to all tissues in the body. Changes in posture create changes in ocular perfusion pressure (OPP) induced by gravity. Therefore, the local microvasculature of ocular structures has to compensate for the altered OPP and altered metabolic stimuli.

Recent studies have investigated the influence of posture change on choroidal BF (ChBF) in normal subjects by using laser doppler flowmetry (LDF).[1,2] Their results have suggested a linear relationship between subfoveal ChBF and OPP, indicating that the vascular bed responds passively to increases in OPP.

The response of retinal and optic nerve head (ONH) circulation to posture change in normal subjects has also been studied with a variety of techniques.[3–7] An autoregulatory response in retinal

Received 10 September 2012; revised 17 November 2012; accepted 10 December 2012; published online 6 May 2013

Correspondence: Toru Nakazawa, MD, PhD, Department of Ophthalmology, Tohoku University Graduate School of Medicine, 1-1, Seiryo, Aoba, Sendai Miyagi: 980-8574, Japan. Tel: +81-22-717-7294. Fax: +81-22-717-7298. E-mail: ntoru@oph.med.tohoku.ac.jp

and ONH BF seems to occur despite variations in OPP. Due to technical limitations, however, conventional instruments have only a small capture area, making it hard to simultaneously obtain images and evaluate differing hemodynamics in the ONH, retinal vessels and choroidal circulation.

Laser speckle flowgraphy (LSFG), by contrast, allows us to make the necessary simultaneous quantification of microcirculation in the ONH, the choroid at the fovea, and the retinal vessels. It is a non-contact technique based on the laser speckle phenomenon, and has been shown to be reliable and reproducible.[8,9] Most importantly, LSFG takes just a few seconds to acquire an image of ocular circulation, and it can be used in living eyes.[8] This quick acquisition of images enables researchers to measure dynamic changes in ONH BF and ChBF during posture change over a shorter period.

This study used LSFG to simultaneously examine dynamic changes in ONH BF and ChBF in normal subjects during the change from a sitting to a supine position, and used the resulting data to compare vascular autoregulation in these two regions.

MATERIALS AND METHODS

Subjects

This study comprised twenty healthy, non-smoking subjects (age: 30.0 ± 8.5 years old, male: female = 15:5), recruited from volunteers at Tohoku University Hospital, Miyagi, Japan. All subjects included in this study had baseline intraocular pressure (IOP) in both eyes below 22 mmHg, as measured by Goldmann applanation tonometry, and normal findings on a slit lamp or funduscopic examination, as well as refractive error within a range of −8.75 to +0.25 diopter (mean: −3.10 ± 2.83), and pupillary diameters measurable by LSFG-NAVI without mydriasis. Subjects were excluded if they had a history of ophthalmic or general disorders, ocular laser or incisional surgery in either eye, or systemic or topical medication. All subjects abstained from alcohol and caffeine for at least six hours before the measurements.

This study monitored only the left eyes of each participant. The local ethics committee approved the procedures and followed the tenets of the Declaration of Helsinki. All participants gave their informed consent before starting the study.

Measurement of Clinical Parameters

Both systemic blood pressure and heart rate (HR) were appropriately measured in the left brachial artery at the height of the heart by an automated blood pressure monitor (HEM-759 E, Omron Corporation, Kyoto, Japan). Mean arterial pressure (MAP) was calculated from systolic blood pressure (sBP) and diastolic blood pressure (dBP) according to the formula: MAP = dBP + 0.42 (sBP − dBP).[1,2,10]

Baseline IOP was determined using Goldmann applanation tonometry, with subjects in a sitting position. IOP in a supine position was measured with a handheld tonometer (Tonopen; Mentor, Norwell, MA).

OPP in a sitting position was calculated according to the formula: $OPP_{sitting} = 2/3\ MAP_{sitting} - IOP$, which accounts for the drop in blood pressure between the brachial and ophthalmic artery when the subject is sitting.[11] The OPP in a supine position was calculated from following equation: $OPP_{supine} = MAP_{supine} - IOP$[4] Since preliminary experiments on five healthy volunteers had shown that there was no significant IOP difference after 2 or 10 min in a supine position (14.8 ± 1.6, 15.4 ± 1.7 mmHg, respectively, $p = 0.55$), and to avoid the influence of anesthesia on the ocular circulation, IOP was not recorded during the 2 min measurements taken in a supine position over the course of 10 min. IOP for the supine position was measured after the full 10 min, and this measurement was substituted for the 2 min measurements when OPP_{supine} was calculated.

LSFG

We assessed ocular circulation BF using the MBR, which we measured using a newer, non-invasive version of LSFG (LSFG-NAVI Softcare., Iizuka, Japan). This instrument consists of a fundus camera equipped with a diode laser (wavelength 830 nm), and an ordinary charge-coupled device (CCD) camera (750 (width) × 360 (height) pixels). The mechanism of LSFG has been described in detail elsewhere.[12,13] MBR was determined using the pattern of speckle contrast produced by the interference of a laser scattered by blood cells moving in the ocular fundus. This is known to be closely associated with BF velocity.[14] The relative velocity of BF can be derived from the inverse of speckle contrast values using computationally intensive calculations.[15] We determined the MBR ratio by normalizing the values measured in a supine position to the baseline (measured in a sitting position) for each subject. The device acquired images of the BF map continuously at the rate of 30 images per second. We analyzed the data from a 5 s time period.[8]

A composite map of BF was obtained at the ONH and the fovea, and the equipped software automatically calculated the MBR in arbitrary units (au) for each area (Figure 1). As depicted in Figure 1, the MBR in the ONH included measurements for the large vessel and capillary areas. This study examined only the

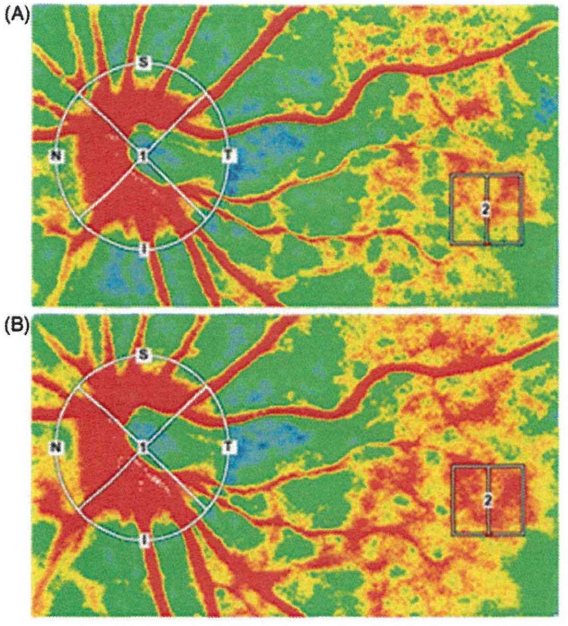

FIGURE 1. Representative retinal images of ocular BF, taken using LSFG, in a sitting position (A) and after 6 min in a supine position (B). The color-coded areas around the ONH (white circle #1) and on the fovea (white square #2) are automatically tracked in the images at each time point.

MBR in the large vessel area of the ONH. The MBR in the fovea was obtained from an area within the fovea one disc diameter in size (150×150 pixels).[9,16] As shown in Figure 2, we used a raised platform specially designed for the safety of the subjects to measure the MBR in a supine position.

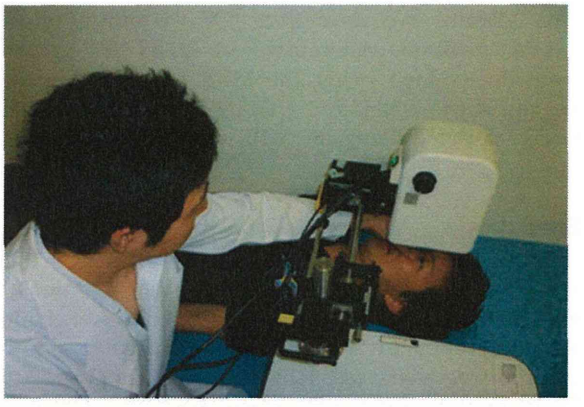

FIGURE 2. A raised platform specially designed in the consideration of patients' safety was used to measure the MBR in the supine position.

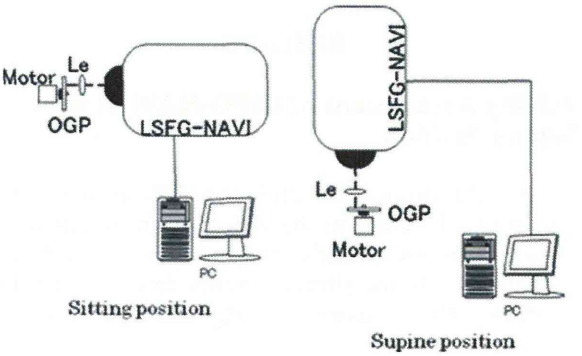

FIGURE 3. Schematic view of the experimental set up for the evaluation of the LSFG-NAVI system's validity. A rotating opal glass (OGP) is located in front of the lens (Le).

Experimental Protocols

Validity Assessment of LSFG-NAVI in the Supine Position

To assess the validity of LSFG-NAVI measurements in the supine position, we compared variations between the MBR and velocity in both the sitting and supine positions. Figure 3 shows the schematic view of the experimental set up with the LSFG-NAVI system. Following a previous study,[17] the rotating opal glass plate (OGP) was placed in front of the LSFG-NAVI system's objective lens (Le), and its movement speed was assumed to be the change in BF velocity. The MBR was obtained by changing the speed of the OGP for each position, and then evaluating whether there were any significant differences in the regression equations of the variation between the MBR and the velocity of the OGP.

Reproducibility Assessment of LSFG-NAVI in the Supine Position

To assess the intrasession reproducibility of LSFG-NAVI measurements in the supine position, we performed a preliminary experiment on ten healthy subjects (20 eyes, mean age: 27.9 ± 5.7 years old; male: female = 5:5). Two parameters indicating reproducibility, the coefficient of variation (COV) and intraclass correlation coefficient (ICC), were evaluated with MBR measurements obtained using LSFG-NAVI during three continuous examinations, on the same day, after 10 min in a supine position.

Testing Protocol

On the day of the test, following a slit lamp examination, a funduscopic examination and baseline IOP measurement taken with Goldmann applanation tonometry, each subject was asked to sit in an upright position for 10 min in a dark room before further investigation. SBP, dBP and HR were then recorded, and the MBR was assessed in a sitting position, to be used as the baseline measurement. Soon after, the subject was asked to lie down on a bed, and sBP, dBP and HR were recorded just before an LSFG measurement was taken, this was repeated every 2 min for the

next 10 min. We measured IOP 10 min after the supine position. Alterations in ONH BF velocity were determined using the MBR ratio in the large vessels of the ONH, and alterations in ChBF velocity were evaluated using the MBR ratio at the fovea.

Statistics

All data are shown as mean ± standard deviation. We used an analysis of covariance to determine any differences in the regression equations of the variation between the MBR and the velocity of the OGP for the sitting and supine positions. Wilcoxon signed-rank tests were applied to assess differences in the measurements for different body positions. The significance level was set at $p<0.05$.

RESULTS

Validity Assessment of LSFG-NAVI in the Supine Position

Figure 4(A) shows variation in the MBR relative to the velocity of the OGP, in the sitting position. The MBR value increases linearly with increasing velocity. Figure 4(B) shows similar results from the supine position. There were no significant differences between the regression equations for each position ($p=0.60$).

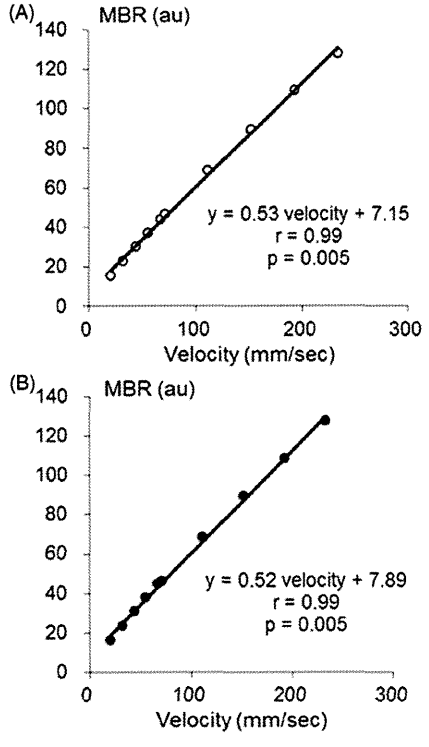

FIGURE 4. The variation in MBR against the velocity of the OGP in the sitting (A) and supine (B) positions.

Reproducibility of LSFG-NAVI in the Supine Position

Reproducibility of LSFG-NAVI was similar in the large vessel area of the ONH and the choroid (large vessel area: COV: 6.72 ± 5.11%, ICC: 0.90; choroid: COV: 7.46 ± 5.81%, ICC: 0.95).

Alteration of Systemic Blood Pressure in Response to Posture Change

In a sitting position, sBP and dBP were 124.9 ± 11.2 mmHg and 76.1 ± 15.0 mmHg, respectively. After the posture change to a supine position, both sBP and dBP did not alter for 2 min. After that, sBP gradually decreased and was statistically significantly lower than the initial sBP (in a sitting position). There was a significant decrease in dBP at four and 6 min after the posture change, after which it returned to the initial level (Figure 5A). The time course of MAP was calculated from sBP and dBP and is depicted in Figure 5(B). The alteration in MAP after the posture change was similar to that in sBP.

Alteration of IOP and OPP in Response to Posture Change

In a sitting position, IOP was 13.4 ± 2.3 mmHg. IOP in a supine position increased significantly to 16.3 ± 2.5 mmHg after 10 min (Figure 5C). The time course for OPP was calculated from MAP and IOP, and is depicted in Figure 5(D). In a sitting position, OPP was 51.0 ± 7.1 mmHg. Two minutes after the posture change, OPP first increased significantly, to 78.5 ± 11.6 mmHg, and then gradually decreased. After 10 min, it was still higher than the baseline, at 74.8 ± 9.8 mmHg.

Alteration of MBR in Response to Posture Change

In a sitting position, the MBR in the vessel area of the ONH was 45.4 ± 7.3 au. The MBR ratio was defined as 100% in each subject. After the posture change, the MBR ratio in the vessel area of the ONH gradually rose, reaching 104.4 ± 5.6% at 4 min, a significant increase, but soon decreased to the initial level, after 6 min (Figure 6A). The MBR in the choroid was 12.2 ± 4.0 au. Two minutes after the posture change, the MBR ratio suddenly rose to 113.7 ± 8.1%, and

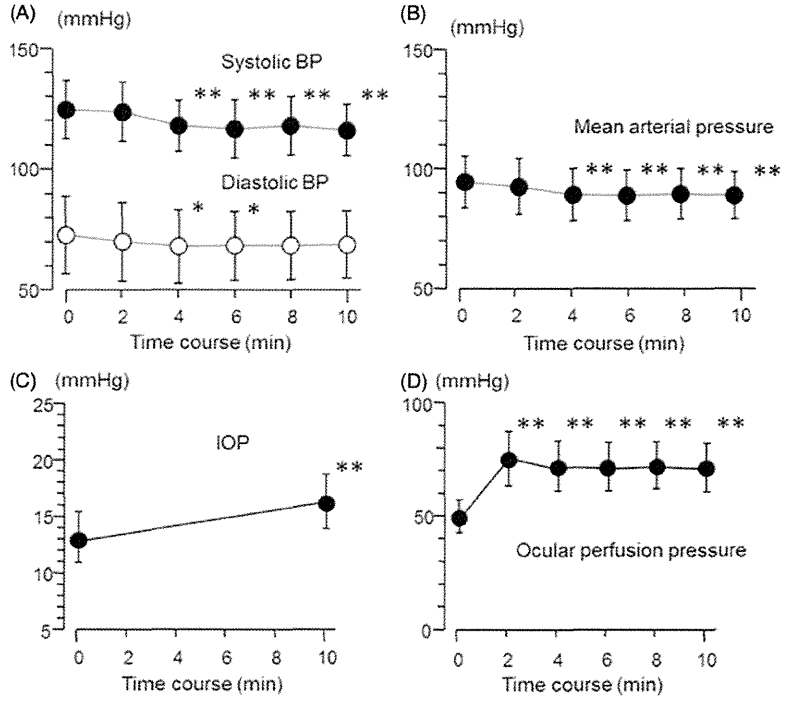

FIGURE 5. Dynamic changes in systolic (●) and diastolic (○) blood pressure in response to a change in posture from a sitting (0 min) to supine position (A). Dynamic changes in MAP (B), IOP (C), and OPP (D) are also depicted. The asterisk indicates a statistically significant difference from the initial sitting position. (Wilcoxon signed-rank tests. *: $p<0.05$. **: $p<0.01$).

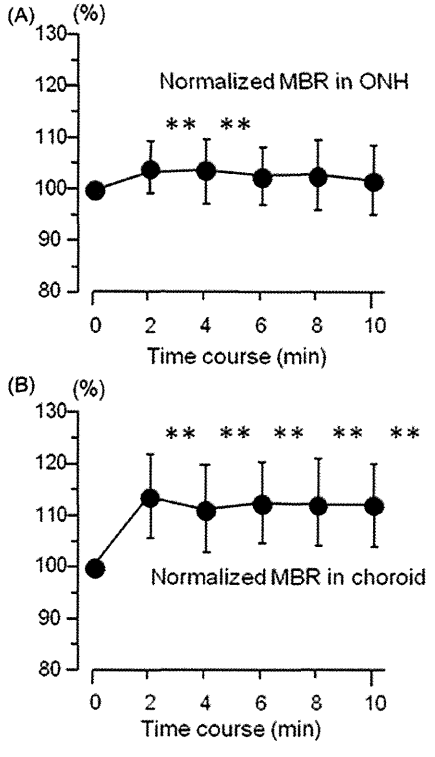

FIGURE 6. The dynamic change in MBR, normalized to the initial sitting position, at the ONH (A) and on the fovea (B) after a posture change to a supine position. The asterisk indicates a statistically significant difference from the initial sitting position. (Wilcoxon signed-rank tests. *: $p<0.05$. **: $p<0.01$).

stayed at this significantly increased level for the entire time course of 10 min (Figure 6B).

DISCUSSION

The authors first evaluated the validity and reproducibility of LSFG-NAVI in the supine position. Variation in the MBR was found to have a linear relationship with the velocity of the OGP in various positions. This result is consistent with previous research.[17] In addition to the validity assessment, we also tested the reproducibility of LSFG-NAVI in the supine position. Our group has previously reported on the reproducibility of determining MBR using LSFG-NAVI in the sitting position in patients with glaucoma or preperimetric glaucoma (COV: 1.9 ± 1.1–$12.4 \pm 12.4\%$; ICC: 0.82–0.98).[9] Results from this regarding the reproducibility of MBR in the supine position are similar to the previous research. As mentioned above, LSFG shows favorable reproducibility in the vessel area of the ONH and choroid in both the supine and sitting positions. This suggests that this instrument is suitable for monitoring changes in ocular circulation in response to posture change.

The major finding of this study is that the dynamic change in BF velocity after posture change, as measured by LSFG-NAVI, differs between the large vessel area of the ONH and the choroidal vessels in normal subjects. Posture change caused a prompt

and continuous increase in OPP for 10 min. In the ONH, a slight increase in BF velocity after posture change was observed within 4 min and was corrected within 6 min.

The large vessel area of the ONH, which we measured with LSFG-NAVI, is thought to be composed mainly of retinal arterial and venous circulation, but LSFG cannot measure retinal and choroidal circulation separately due to technical limitations.[8]

The finding that ONH BF velocity increases significantly after 2 min indicates that it compensates for retinal vessel responses to posture change.

Several studies of regulation in the retinal vasculature in response to isometric exercise and posture change have suggested that an increase in systemic blood pressure or retinal perfusion pressure induces a vasoconstrictive response in the retinal arterioles.[3,18–20] Baer and Hill[5] have reported that the caliber of the retinal arteries decreased significantly, with a corresponding increase in the caliber of the retinal veins, approximately 90 s after tilting the head to a bowed position. That reports tends to support the premise of this author.

The finding that velocity in the ONH returned to the initial level after only 6 min, despite a continuous increase in OPP, indicates the existence of an autoregulatory mechanism that begins working within several minutes.

Generally, there are thought to be both myogenic and metabolic components to the mechanism of retinal BF autoregulation.[21] The myogenic component is defined as the response of the vascular smooth muscle and endothelial cells to mechanical forces, and this response may require several minutes to induce stable vessel diameters following an acute change in intravascular pressure.[22,23] By contrast, the metabolic component is the interaction of factors released from neurons and glial cells, which affects vascular smooth muscle cells and pericytes and changes the tone of vascular resistance. This response seems to occur within a few seconds.[24] Our results showed that the autoregulatory mechanism for ONH BF was complete after 6 min, meaning that our results for dynamic change possibly reflect the myogenic mechanism.

Ocular BF depends on the interaction of various factors, such as the vascular resistance generated by the diameter and length of the vessels, and blood viscosity. In this study, changes in these factors due to posture change were not measured due to the technical difficulty involved, but in the future, a simultaneous evaluation of OPP and these factors should be done to assess the driving force of BF.

In this study, the authors also measured the MBR in the choroid at the fovea, which is thought to reflect over 90% of the ChBF.[13] In the choroid, a significant increase in BF velocity was observed within 2 min, and was sustained for 10 min. This was synchronized with OPP dynamics. Since choroidal circulation is mainly controlled by sympathetic innervation and is not autoregulated,[25] it has been believed that ChBF responds passively to changes in OPP.[1,2] Our finding of an approximately 14% increase in the MBR ratio in the choroid is similar to the 11% increase in ChBF reported by Longo[1], although the two investigations differ in that our study used LSFG and focused on the period between 2 and 10 min after posture change, and the latter study used LDF and focused on the 2 min period after posture change. In this study, as in previous studies, dynamic change in the choroid correlated with OPP, suggesting a lack of autoregulation.

According to recent studies of retinal and ChBF, there is considerable evidence that vascular dysregulation in eyes with glaucoma[26–29] or diabetic retinopathy[30] occurs in the subclinical stages of these diseases. Recent studies have demonstrated that LSFG enables us to assess alterations in the autoregulation of ONH BF in experimental animals.[31,32] To the best of our knowledge, however, no information has yet been available on the use of LSFG-NAVI in human beings to assess changes in ocular circulation in response to posture change. The authors can confirm that this new approach for evaluating hemodynamics in ONH BF and ChBF in response to posture change using LSFG-NAVI may be useful in screening for certain eye diseases, due to its quick and easy acquisition of wide angle images of the retina. Our data accords with previous studies reporting that IOP increases significantly with a postural change from a sitting to a supine position,[33,34] Furthermore, the magnitude of the IOP elevation was higher in patients with glaucoma than in controls, which may indicate an association with glaucomatous damage.[35–37] Therefore, both vascular dysregulation and IOP change may be associated with the development and progression of glaucomatous change. Of course, we acknowledge the limitations of this study, which had only a small number of normal subjects. In the future, larger, multi-center studies using subjects with eye disease, particularly those with glaucoma, must be performed.

In conclusion, LSFG-NAVI showed favorable validity and reproducibility in both the supine position and the sitting position, suggesting that this instrument is suitable for monitoring changes in ocular circulation in response to posture change. Additionally, we investigated the dynamic response of ONH BF and ChBF to posture change in an intermediate time frame (2–10 min) of the vasculature's adaptation, allowing us to obtain similar results to previous studies.

ACKNOWLEDGEMENTS

The authors thank Tim Hilts for reviewing the manuscript.

DECLARATION OF INTEREST

There is no financial support to report, and there were no conflicts of interest in this study.

REFERENCES

1. Longo A, Geiser MH, Riva CE. Posture changes and subfoveal choroidal blood flow. Invest Ophthalmol Vis Sci 2004;45:546–551.
2. Kaeser P, Orgul S, Zawinka C, Reinhard G, Flammer J. Influence of change in body position on choroidal blood flow in normal subjects. Br J Ophthalmol 2005;89: 1302–1305.
3. Tachibana H, Gotoh F, Ishikawa Y. Retinal vascular autoregulation in normal subjects. Stroke 1982;13: 149–155.
4. Hague S, Hill DW. Postural changes in perfusion pressure and retinal arteriolar calibre. Br J Ophthalmol 1988;72: 253–257.
5. Baer RM, Hill DW. Retinal vessel responses to passive tilting. Eye (Lond) 1990;4:751–756.
6. Baxter GM, Williamson TH, McKillop G, Dutton GN. Color Doppler ultrasound of orbital and optic nerve blood flow: effects of posture and timolol 0.5%. Invest Ophthalmol Vis Sci 1992;33:604–610.
7. Feke GT, Pasquale LR. Retinal blood flow response to posture change in glaucoma patients compared with healthy subjects. Ophthalmology 2008;115:246–252.
8. Sugiyama T, Araie M, Riva CE, Schmetterer L, Orgul S. Use of laser speckle flowgraphy in ocular blood flow research. Acta Ophthalmol 2010;88:723–729.
9. Aizawa N, Yokoyama Y, Chiba N, Omodaka K, Yasuda M, Otomo T, et al. Reproducibility of retinal circulation measurements obtained using laser speckle flowgraphy-NAVI in patients with glaucoma. Clin Ophthalmol 2011;5: 1171–1176.
10. Sayegh FN, Weigelin E. Functional ophthalmodynamometry. Comparison between brachial and ophthalmic blood pressure in sitting and supine position. Angiology 1983;34: 176–182.
11. Riva CE, Grunwald JE, Petrig BL. Autoregulation of human retinal blood flow. An investigation with laser Doppler velocimetry. Invest Ophthalmol Vis Sci 1986;27: 1706–1712.
12. Tamaki Y, Araie M, Kawamoto E, Eguchi S, Fujii H. Noncontact, two-dimensional measurement of tissue circulation in choroid and optic nerve head using laser speckle phenomenon. Exp Eye Res 1995;60:373–383.
13. Isono H, Kishi S, Kimura Y, Hagiwara N, Konishi N, Fujii H. Observation of choroidal circulation using index of erythrocytic velocity. Arch Ophthalmol 2003;121: 225–231.
14. Fujii H, Nohira K, Yamamoto Y, Ikawa H, Ohura T. Evaluation of blood flow by laser speckle image sensing. Part 1. Appl Opt 1987;26:5321–5325.
15. Briers JD, Fercher AF. Retinal blood-flow visualization by means of laser speckle photography. Invest Ophthalmol Vis Sci 1982;22:255–259.
16. Tamaki Y, Araie M, Tomita K, Nagahara M, Tomidokoro A, Fujii H. Real-time measurement of human optic nerve head and choroid circulation, using the laser speckle phenomenon. Jpn J Ophthalmol 1997;41:49–54.
17. Konishi NTY, Kohra K, Fujii H. New laser speckle flowgraphy system using CCD camera. Opt Rev 2002;9: 163–169.
18. Blum M, Bachmann K, Wintzer D, Riemer T, Vilser W, Strobel J. Noninvasive measurement of the Bayliss effect in retinal autoregulation. Graefes Arch Clin Exp Ophthalmol 1999;237:296–300.
19. Nagel E, Vilser W. Autoregulative behavior of retinal arteries and veins during changes of perfusion pressure: a clinical study. Graefes Arch Clin Exp Ophthalmol 2004; 242:13–17.
20. Jeppesen P, Gregersen PA, Bek T. The age-dependent decrease in the myogenic response of retinal arterioles as studied with the Retinal Vessel Analyzer. Graefes Arch Clin Exp Ophthalmol 2004;242:914–919.
21. Pournaras CJ, Rungger-Brandle E, Riva CE, Hardarson SH, Stefansson E. Regulation of retinal blood flow in health and disease. Prog Retin Eye Res 2008;27:284–330.
22. Halpern W, Osol G. Influence of transmural pressure of myogenic responses of isolated cerebral arteries of the rat. Ann Biomed Eng 1985;13:287–293.
23. Rajagopalan S, Dube S, Canty Jr JM. Regulation of coronary diameter by myogenic mechanisms in arterial microvessels greater than 100 microns in diameter. Am J Physiol 1995; 268:H788–H793.
24. Florence G, Seylaz J. Rapid autoregulation of cerebral blood flow: a laser-Doppler flowmetry study. J Cereb Blood Flow Metab 1992;12:674–680.
25. Delaey C, Van De Voorde J. Regulatory mechanisms in the retinal and choroidal circulation. Ophthalmic Res 2000;32: 249–256.
26. Evans DW, Harris A, Garrett M, Chung HS, Kagemann L. Glaucoma patients demonstrate faulty autoregulation of ocular blood flow during posture change. Br J Ophthalmol 1999;83:809–813.
27. Fuchsjager-Mayrl G, Wally B, Georgopoulos M, Rainer G, Kircher K, Buehl W, et al. Ocular blood flow and systemic blood pressure in patients with primary open-angle glaucoma and ocular hypertension. Invest Ophthalmol Vis Sci 2004;45:834–839.
28. Galambos P, Vafiadis J, Vilchez SE, Wagenfeld L, Matthiessen ET, Richard G, et al. Compromised autoregulatory control of ocular hemodynamics in glaucoma patients after postural change. Ophthalmology 2006;113: 1832–1836.
29. Ulrich A, Ulrich C, Barth T, Ulrich WD. Detection of disturbed autoregulation of the peripapillary choroid in primary open angle glaucoma. Ophthalmic Surg Lasers 1996;27:746–757.
30. Burgansky-Eliash Z, Nelson DA, Bar-Tal OP, Lowenstein A, Grinvald A, Barak A. Reduced retinal blood flow velocity in diabetic retinopathy. Retina 2010;30: 765–773.
31. Liang Y, Downs JC, Fortune B, Cull G, Cioffi GA, Wang L. Impact of systemic blood pressure on the relationship between intraocular pressure and blood flow in the optic nerve head of nonhuman primates. Invest Ophthalmol Vis Sci 2009;50:2154–2160.
32. Shibata M, Oku H, Sugiyama T, Kobayashi T, Tsujimoto M, Okuno T, et al. Disruption of gap junctions may be involved in impairment of autoregulation in optic nerve head blood flow of diabetic rabbits. Invest Ophthalmol Vis Sci 2011;52:2153–2159.
33. Anderson DR, Grant WM. The influence of position on intraocular pressure. Invest Ophthalmol 1973;12: 204–212.
34. Tsukahara S, Sasaki T. Postural change of IOP in normal persons and in patients with primary wide open-angle glaucoma and low-tension glaucoma. Br J Ophthalmol 1984;68:389–392.
35. Kiuchi T, Motoyama Y, Oshika T. Relationship of progression of visual field damage to postural changes

in intraocular pressure in patients with normal-tension glaucoma. Ophthalmology. 2006;113:2150–2155.
36. Kiuchi T, Motoyama Y, Oshika T. Postural response of intraocular pressure and visual field damage in patients with untreated normal-tension glaucoma. J Glaucoma 2010;19:191–193.
37. Mizokami J, Yamada Y, Negi A, Nakamura M. Postural changes in intraocular pressure are associated with asymmetrical retinal nerve fiber thinning in treated patients with primary open-angle glaucoma. Graefes Arch Clin Exp Ophthalmol 2011;249: 879–885.